Unravelling the atomic structure of AgInSbTe phase change materials: Theoretical perspective

J. Akola[1,2,3] and R.O. Jones[3,4]

[1]Department of Physics, Tampere University of Technology, P.O. Box 692, FI-33101, Tampere, Finland

[2]Nanoscience Center, Department of Physics, P.O.Box 35, FI-40014 Jyväskylä, Finland

[3]Institut für Festkörperforschung, Forschungszentrum Jülich, D-52425 Jülich, Germany

[4]German Research School for Simulation Sciences, FZ Jülich and RWTH Aachen University, D-52425 Jülich, Germany

jaakko.akola@tut.fi,   r.jones@fz-juelich.de

ABSTRACT

Phase change (PC) optical memories are based on the astonishingly rapid (nanosecond scale) crystallization of nanosized amorphous "marks" in a polycrystalline layer. Until recently, models of crystallization existed for the PC alloy $Ge_2Sb_2Te_5$ (GST), but not for the important class of Sb-Te based alloys. We have performed density functional simulations on amorphous and crystalline $Ag_{3.5}In_{3.8}Sb_{75.0}Te_{17.7}$ (AIST). The combination with experiment (XRD, EXAFS, hard x-ray photoelectron spectroscopy) has enabled us to determine their structures and how they differ from GST [1]. We focus here on the theoretical aspects and present some additional information. Amorphous (a-) AIST has a range of ring sizes, while a-GST has many small rings and cavities, and the local environment of Sb in both forms of AIST is a distorted 3+3 octahedron. We propose a "bond interchange" model (a sequence of small displacements of Sb atoms accompanied by interchanges of short and long bonds) as the origin of the rapid (slow nucleation) crystallization of a-AIST. It differs profoundly from crystallization in a-GST.

Key words: phase change materials, Ag/In/Sb/Te alloys, density functional, molecular dynamics

1. INTRODUCTION

Phase change (PC) materials are chalcogenide alloys that switch very rapidly between the amorphous (a-) and crystalline (c-) phases. They are used extensively in rewritable high-density data storage, especially in optical recording [Digital Versatile Disc (DVD), Blu-ray Disc] [2]. Information is stored as a row of nanosized amorphous marks in a polycrystalline layer or cell arrays and accessed via the difference between optical or electrical properties in the two phases. The most common materials are $GeTe-Sb_2Te_3$ pseudobinary compounds (Group 1 in Fig. 1a) and Sb-Te binary compounds with small amounts of In, Ag, and/or Ge, e.g. $Ag_{3.5}In_{3.8}Sb_{75.0}Te_{17.7}$ (AIST), shown as Group 2 in Fig. 1a. Recrystallization in the two groups is strikingly different: In Group 1 it proceeds mainly via nucleation inside the marks (Fig. 1b), in Group 2 via crystal growth from the rim (Fig. 1c) [2].

Materials in both groups have superior rewrite speeds, and their amorphous phases are stable at room temperature (RT) for long periods, indispensable characteristics of PC memories. Elements in groups V and VI (including As, Sb, S, Se, and Te) readily form disordered structures that are often short-lived at RT, but compounds containing other elements, such as Ag and In or Ge, can remain amorphous at RT for several decades. High stability implies a low tendency to crystallize, but this process can be accelerated greatly by laser irradiation or electric heating. Crystallization of amorphous $Ge_2Sb_2Te_5$ (GST) and AIST materials can occur within tens of nanoseconds [3], so they have both the long-term stability and the rapid switching needed for effective PC memories. An atomic understanding of crystallization is essential, as it is the rate-limiting process in all PC materials.
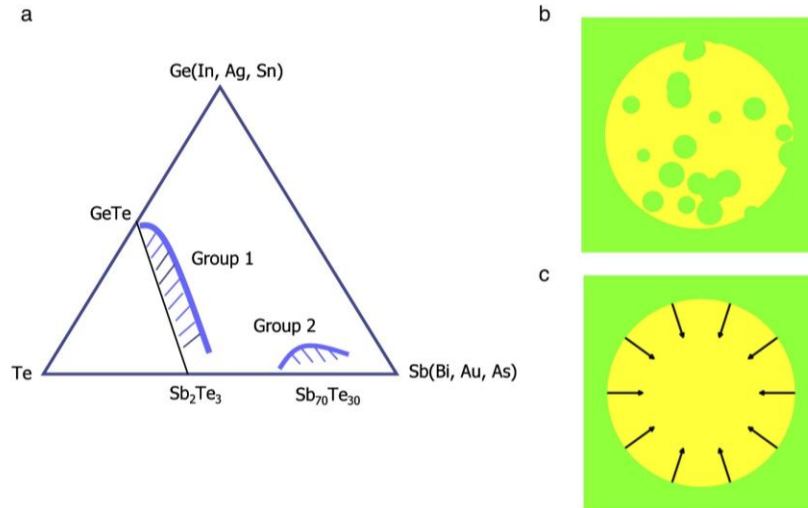
Figure 1. PC materials and their crystallization patterns. (a) The most commonly used materials for optical recording are in Groups 1 and 2. (b) Nucleation-dominated recrystallization (as in GST), (c) Growth-dominated recrystallization (AIST).

There have been many studies of crystalline GST (rock salt) and AIST (A7) materials [2]. The average number of *p*-electrons is near 3 in all compositions, suggesting orthogonal bonds with neighbouring atoms and octahedral coordination. Such structures are spatially isotropic or have near cubic symmetry, examples being high-temperature structures of AIST crystals [4]. Much less is known about the structure of the amorphous phases, so that the PC mechanism remains the subject of speculation. There have been numerous studies on a-GST recently, including the combination of density functional (DF) / molecular dynamics (MD) and reverse Monte Carlo (RMC) simulations we used to reproduce x-ray diffraction (XRD) and hard x-ray photoelectron spectroscopy (HXPS) data. The structure of a-GST has many small rings with "*AB* alternation" (*A*: Ge, Sb; *B*: Te) that act as nuclei in the crystallization process [5]. However, little is known about the amorphous structures of Group 2 materials, including AIST. The technique used for a-GST [experiment (XRD, HXPS, and EXAFS) combined with DF/MD simulations] has been applied to determine the a- and c-structures of an AIST alloy, $Ag_{3.5}In_{3.8}Sb_{75.0}Te_{17.7}$. The differences between the structures of GST (Group 1) and AIST (Group 2) have wider implications.

2. DENSITY FUNCTIONAL CALCULATIONS AND RMC REFINEMENT

The combined DF/MD calculations were performed with the CPMD package [6], using the approximation of Perdew *et al.* (PBEsol) [7] for the exchange-correlation energy and Troullier-Martins pseudopotentials [8] (with non-linear core corrections). The valence states of Ag and In included the 4*d* electrons. Periodic boundary conditions were used, with a single point (*k*=0) in the Brillouin zone. The kinetic energy cutoff of the plane wave basis was 60 Ry, and Born-Oppenheimer simulations were performed with time steps of 3.025 fs and 6.050 fs for initialization and data collection, respectively. The unit cell contained 23 Ag, 25 In, 480 Sb, and 112 Te atoms, with densities of 0.0329 atoms/$Å^3$ (c-AIST) and 0.0306 atoms/$Å^3$ (a-AIST). The simulations started at 3000 K (liquid) in a cubic box (side 27.09 Å), followed by cooling (30 ps) to the melting point (850 K, 0.0322 atoms/$Å^3$) and data collection (20 ps) [9]. Cooling to 300 K over 100 ps with gradually decreasing density was then followed by data collection (30 ps) and quenching. The geometry was optimized at the final density (box size 27.57 Å) and refined using the RMC++ code [10] with the experimental x-ray total structure factor *S*(*Q*) and constraints on (a) the average coordination number of all atoms and (b) the distributions of bond angle distributions Sb-Sb-Sb, Sb-Te-Sb, Te-Sb-Sb and Te-Sb-Te.

The calculations on c-AIST (A7 structure) used 648 atoms in a hexagonal unit cell (*a*=25.826 Å, *c*=33.43 Å). The lattice sites were occupied by 23 Ag, 25 In, 486 Sb, and 114 Te atoms by introducing correlations between minority atoms (Ag, In) and Te (Ag/In attracted by Te, Te avoids itself) and optimizing the structure. A cutoff distance of 3.2 Å was applied to analyze PDF and angular and ring distributions, and the electronic structure was analyzed using atom-

centred orbitals and Mayer bond orders. The cavity analysis [11] used a test particle with cutoff radius 2.8 Å. The cohesive energy is 35 meV/atom lower in a-AIST than in c-AIST (4.07 eV/atom).

The presence of four elements and the dominance of two (Sb, Te) with similar atomic numbers rule out determining the local structure of AIST by XRD alone, so that we have performed a melt-quenched DF simulation of a-AIST (640 atoms) and refined the structure using a reverse Monte Carlo (RMC) method. The criteria were: (a) agreement with XRD data, (b) a total energy close to the DF minimum, and (c) agreement with the HXPS measurements of electronic structure. The second and third requirements required carefully chosen constraints on bond distances and bond angles, but the resulting $S(Q)$ and $T(r)$ agreed very well with experiment (blue lines in Figs. 2a-b). AIST and GST geometries are shown in Figs. 2c and 2d, respectively. The total energy of RMC-refined a-AIST is only 68 meV/atom above the lowest DF energy. The minority atoms (48 Ag and In atoms in the simulation cell) seldom bind to each other (see Fig. 2c), but often bind to Te (Te avoids itself), suggesting that AIST may segregate into Sb and $AgInTe_2$ under certain conditions [12]. The local environment of Sb (75% of all atoms) is very similar to that in the crystal (A7, a distorted octahedron). Cavities are small, and their total volume (7%) is much less than in a-GST (14%) [11]. Crystalline AIST has no cavities, c-GST 10%. The difference between the cavities in a-AIST and a-GST is clearly visible in Figs. 2c and 2d, where large cavities are pink. The lower figures in Fig. 2 show that "*ABAB*-squares" [11] with alternating Te and Ge (or Sb) atoms are prevalent in a-GST, but insignificant in a-AIST.

3. RESULTS AND DISCUSSION

Fig. 2a shows the structure factors $S(Q)$ of AIST and GST obtained using XRD [13]. Both c-forms have sharp Bragg peaks (red lines), and the a-forms (black lines) have typical halo patterns. However, oscillations up to the maximum Q value in a-AIST indicate a structure with well defined short-range order. Fourier transformation of the $S(Q)$ lead to the total correlation functions $T(r)$ for c-AIST and c-GST (Fig. 2b), which are very similar beyond 4 Å. Small differences exist between the two crystalline forms at shorter distances, e.g. the double peak in c-AIST (2.93 Å and 3.30 Å) and a single peak in c-GST (2.97 Å). The $T(r)$ for the *amorphous* materials, however, differ significantly: the first peak in a-AIST (2.86 Å) is only slightly shorter than that found in c-AIST (2.93 Å), whereas the first peak in a-GST (2.79 Å) is much shorter than that in c-GST (2.97 Å). The shoulder on the second peak in a-AIST (3.5 Å, arrowed) is near that observed in the crystalline form (3.30 Å). These differences provide is strong evidence that the materials crystallize differently. The atomic motion and/or diffusion accompanying the phase change are larger in GST than in AIST, where the phase change is accompanied by small changes in bond lengths.

The DF-RMC structure of a-AIST were compared with the local structure of each element determined by EXAFS measurements at 26 K, and the coordination numbers N and bond lengths r determined (Table 1) agree with those found by Tashiro *et al*. [14] at RT for a similar AIST composition. Table 1 also gives values for the DF-RMC geometry based on the partial pair distribution functions $g_{ij}(r)$ (PDF) and bond order analysis [1]. The coordination numbers from EXAFS measurements for Sb (3.7 ± 0.3) and Te (2.4 ± 0.4) agree well with the calculated values. The dopants Ag and In are more challenging; EXAFS measurements indicate that there are only small differences between the bond lengths, with Ag bonds being slightly shorter (2.80 Å). This is consistent with the DF-RMC results, where the bond lengths are near 2.85 ± 0.05 Å for most PDFs.

Table 1. Local structure of a-AIST determined by EXAFS at 26 K and by DF/MD (RMC-refined DF geometry). N: coordination number, r: nearest neighbour bond lengths, N_{bond}: chemical coordination number (c-AIST value in brackets)

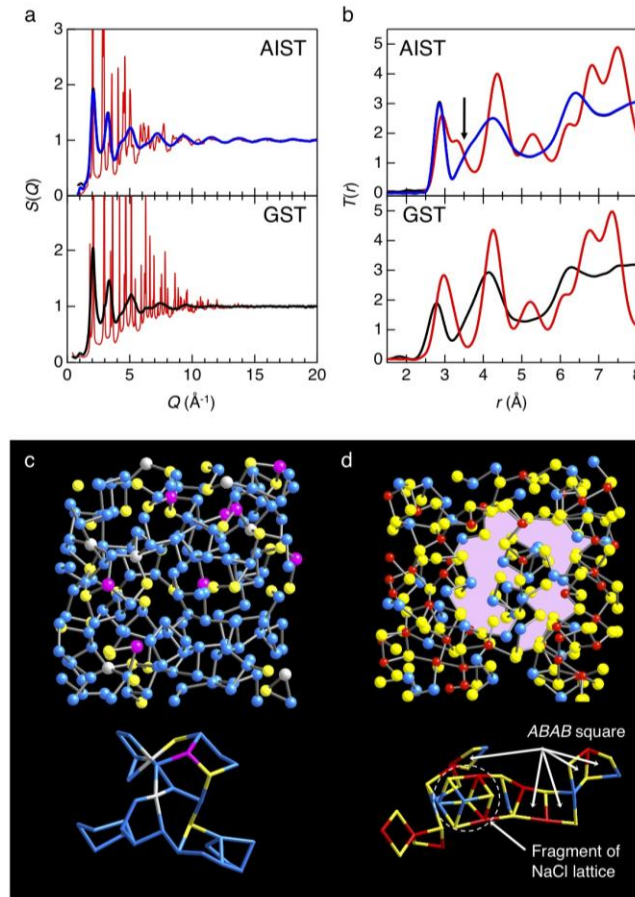| Atom (i)	N_{EXAFS}	r_{EXAFS} (Å)	$N_{DF/MD}$	$r_{DF/MD}$ (Å)	N_{bond}
Ag	3.3 ± 0.5	2.768 ± 0.006	4.4	2.80 ± 0.05	1.9 (2.0)
In	4.3 ± 0.6	2.826 ± 0.006	3.1	2.85 ± 0.05	2.5 (2.9)
Sb	3.7 ± 0.3	2.872 ± 0.006	3.3	2.85 ± 0.05	3.1 (3.2)
Te	2.4 ± 0.4	2.827 ± 0.006	2.5	2.85 ± 0.05	2.5 (2.6)

Figure 2. HEXRD data for AIST and GST, and atomic configurations of a-AIST and a-GST. (a-b) $S(Q)$ and $T(r)$ of AIST and GST [5]. Red line: experimental data of c-phase, black line: experimental data of a-phase, blue line: DF-RMC model of a-AIST. The DF-RMC and experimental results are practically indistinguishable. (c) Part of 640 atom model of a-AIST (24 Å x 24 Å x 12 Å). Ag, silver; In, magenta; Sb, blue; Te, yellow. (d) Part of 460 atom model of a-GST Å (24 Å x 24 Å x 12 Å), Ge, red; Sb, blue; Te, yellow, large cavity, pink.

The DF-RMC structure is consistent with both HEXRD and EXAFS data, and the density of states (DOS) calculated for this structure has been compared with HXPS measurements in Ref. [1]. As in GST [15], the amorphous and crystalline phases of AIST have similar HXPS spectra. The calculated DOS of c-AIST differs in one detail from the HXPS measurements in that there is a non-zero value at the Fermi energy, i.e. the small band gap semiconductor appears to be "metallic". DF calculations of this type focus on total energy differences, and the Kohn-Sham eigenvalues shown here commonly underestimate gaps between occupied and unoccupied states. The orthogonal p^3-type bonds should dominate the bonding in both phases, so that the phase change in AIST could occur by rapid bond interchange involving p electrons with smaller atomic movements than those in GST. This is consistent with small change in the $T(r)$ the XRD data for the two phases, which is not found in GST.

The above comparison with XRD, EXAFS, HXPS data shows that our DF-RMC model of a-AIST describes reliably both the atomic arrangement and the electronic structure. A comparison of bonding in a-AIST and c-AIST is essential to understand the differences in PC mechanism, and DF calculations provide information about the bond order (the number of chemical bonds between pairs of atoms) and the effective atomic charges. These are discussed in detail in Ref. [1]. The chemical coordination numbers N_{bond}, calculated by adding the bond orders to the coordination numbers, provide additional insight (Table 1). The values for Ag, Sb, and Te of a-AIST are almost the same as in c-AIST, e.g. N_{bond} for Sb in a-AIST (3.1) is very close to that in c-AIST (3.2). The bond order profiles of Sb-Sb and Sb-Te are

strikingly similar in a-AIST and c-AIST [1]. The small change in the structure between covalent bonds in a-AIST and resonant bonds [16] in c-AIST should therefore provide adequate optical contrast between them. This situation is similar to that in GST, where angular disorder breaks the resonant bonds in a-GST and provides sufficient optical contrast between a-GST and c-GST [17].
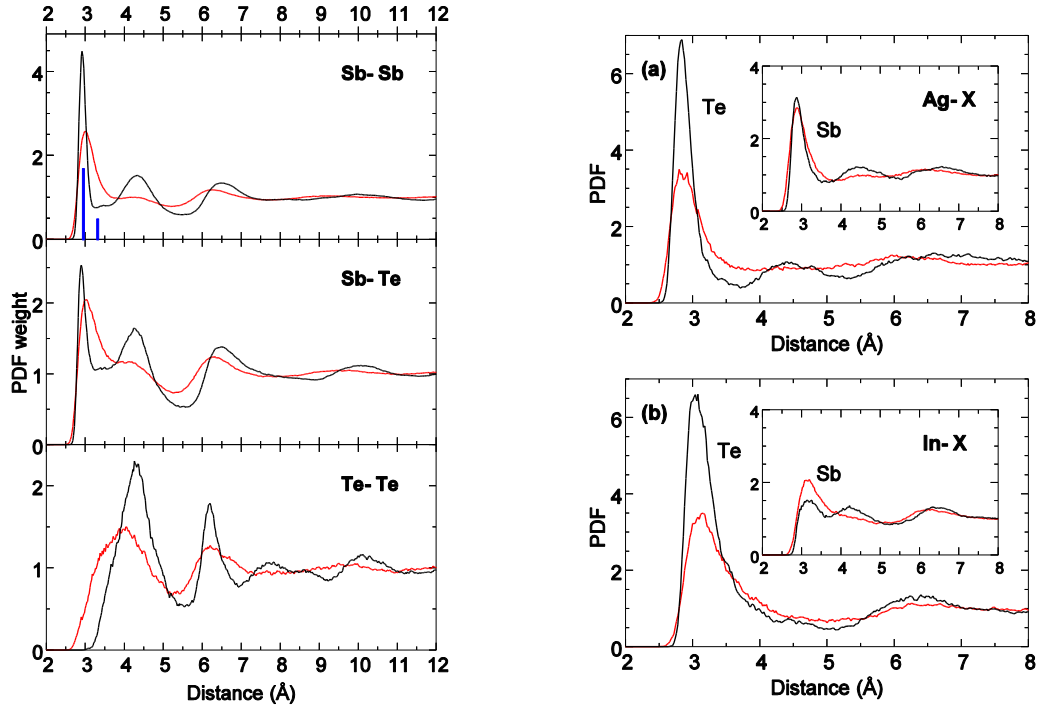

Figure 3. Comparison of PDF for a-AIST (black), liquid AIST (red). The vertical blue lines show values for c-AIST.

In Figure 3 we compare the calculated PDF for the amorphous and liquid [9] phases of AIST. The trends upon cooling are: (1) The first peak of the Sb-Sb and Sb-Te distributions are much sharper in a-AIST, and the bond lengths are close to those of c-AIST (short bonds). Both a- and c-AIST have a second maximum at 4.3 Å, which is consistent with a (pseudo)cubic medium range order. (2) Te-Te bonds are almost absent in a-AIST, while the PDF of c-AIST shows definite medium-range order with an enhanced peak at 6.2 Å. (3) Ag and In prefer to bind to Te, as seen in the stronger first peak for a-AIST after relaxation. We note, in particular, the reduced number of In-Sb bonds.

The structure (bond lengths and angles) and chemical coordination numbers obtained by the RMC-refined DF calculations lead to the local environment around Sb atoms shown in Fig. 4, which shows that both a-AIST (left panel) and c-AIST (right panel) resemble (distorted) 3+3 octahedra. Each vector shown is the sum of (typically three) short bonds and have been computed for each atom by summing bond vectors and applying a smooth Fermi function (cutoff at 3.2 Å) for individual weights. The norm of a vector is largest for three short bonds (orthogonal directions, distorted octahedron), and the vectors are randomly oriented in a-AIST. Laser irradiation or electric heating can lead to a sequence of small atomic shifts that align the vectors along the c_H−axes of crystalline (A7, hexagonal) cells in the rim, so that the entire amorphous mark takes on the A7 structure. We suggest that the phase change is simply a small displacement of the central atom as it interchanges one short (red) and one long (dashed) bond. Here there are three potential bond-pairs in orthogonal directions. The close correspondence between the first peaks in $T(r)$ in a- and c-AIST is further evidence that the structural change is dominated by bond interchanges among near neighbours.

The atomic interchange alters the orientation of the octahedron, which can adapt to the crystalline surroundings. The lower panels of Fig. 4 show how the vectors, randomly oriented in a fragment of a-AIST, become aligned along the c_H-axis. The octahedra order (A7 structure), the cavities disappear, and the density increases by 7%. The small atomic displacement simply interchanges a strong bond and a weak bond, without requiring bond breaking or diffusion. The

process is a sequential, collective motion of Sb atoms, the main component of a-AIST, and an avalanche of bond interchanges is consistent with both the instability of amorphous Sb and the rapid phase change in a-AIST and other Group 2 materials [18].
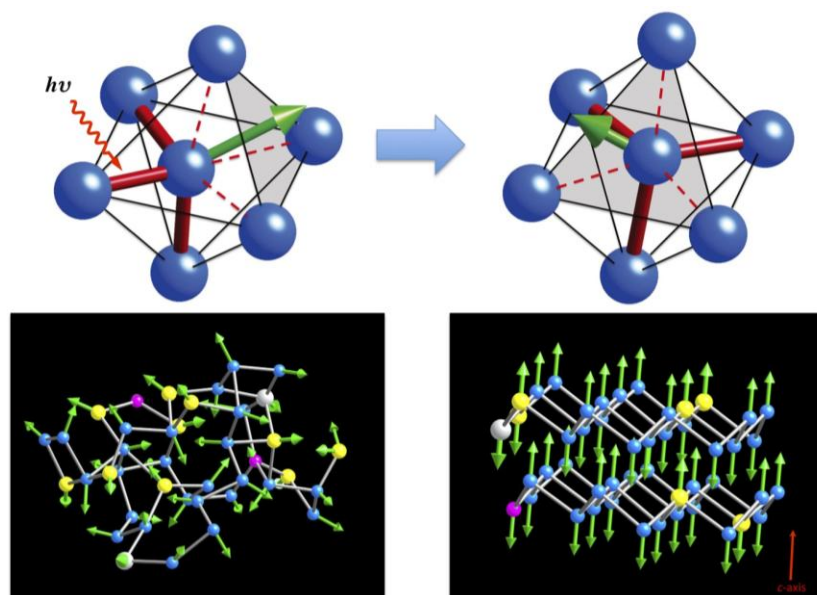

Figure 4. PC mechanism in a-AIST. Laser light excites bonding electrons and causes the atoms to move. The central atom with three short (red) and three long (dashed) bonds moves past the centre of the distorted octahedron, interchanging a short and a long bond. Green: resultant vector of short bonds. The grey sticks (lower right) correspond to the red bonds (upper right). Atom colours as in Fig. 2c.

The structure and electronic properties of a-AIST and a-GST have been determined using identical techniques, and we now discuss their crystallization processes. First, the distributions of closed loops ("ring statistics") differ significantly [1]. In a-GST, 40 % of the rings are 4-fold or 6-fold, while the distribution in a-AIST is much broader; the most common (5-fold) rings make up only 15 % of the total. Amorphous AIST shows links between rings of various sizes (Fig. 2c), while small rings dominate in a-GST (Fig. 2d). Differences in the topological constraints of ring statistics and cavity concentrations in a- and c-GST imply crystallization processes with changes in bond lengths and coordination numbers (see Fig. 2b). In a-AIST, we propose that a sequence of ring reconstructions via bond interchanges results in 6-fold rings with short Sb bonds accompanied by small changes in the bond lengths (see Fig. 2b). Crystallization proceeds either from the crystalline area surrounding an amorphous mark (growth-dominated crystallization) or from a crystalline seed (template) that exceeds the critical size for nucleation (slow nucleation for Group 2). The latter occurs in as-deposited AIST films where the amorphous area is larger, and such films crystallize with difficulty if the surroundings of an amorphous mark are not crystalline [1]. By contrast, many 4- and 6-fold rings in a-GST act as nuclei for crystallization and require larger atomic displacements than in a-AIST. Crystallization starts simultaneously from many such nuclei in the amorphous mark (NaCl fragments, Fig. 2d) and results in small crystal grains. This process is aided by the higher concentrations of cavities (Fig. 2d) and of Te atoms, which favour low coordination. The structures we have found have led us to propose a "bond interchange" model as the origin of "growth-dominated" crystallization of a-AIST, whereas the large fraction of crystalline nuclei in a-GST is the origin of the "nucleation-driven" crystallization in GST. Nucleation is slower in AIST than in GST, because larger crystalline seeds are needed to impose an A7-type director on the neighbouring amorphous atoms.

4. CONCLUSIONS

Extensive experimental (XRD, EXAFS, HXPS) and theoretical (DF/MD simulation with 640 atoms) studies of the AIST alloy $Ag_{3.5}In_{3.8}Sb_{75.0}Te_{17.7}$ have revealed its structure and related properties. The local environment of Sb atoms

resembles a distorted 3+3 octahedron in both c- and a-phases, and the bond lengths in a-AIST are slightly shorter (stronger) than in c-AIST (Fig. 2b, Table 1), with enhanced insulating or semiconducting features. Crystalline AIST has a distorted octahedral structure and more metallic features, as seen in the electronic DOS. The similarity between the DOS in a- and c-phases is consistent with small atomic displacements during the phase change.

According to the above bond-interchange model, crystallization of a-AIST can be viewed as a rapid succession of diffusionless events where the 3+3 octahedra are aligned along the crystalline c_H-axis imposed by the surrounding crystal (see Fig. 1c). Heating or photon excitation causes the octahedra to align near the matrix boundary, and blade- or needle-like crystallites can grow along the laser-scanning direction, as often observed in Sb-based PC materials. The lack of cavities and chemical alternation in a-AIST favour smooth crystal growth. The precise roles of the low-concentration dopant atoms (Ag, In) are not yet clear, but they increase the viscosity at temperatures near RT, impeding atomic motion and stabilizing the amorphous marks. This is consistent with the dopant dependence of the crystallization temperature found in AIST [20]. In a-GST, dominant small-sized rings with chemical alternation ("*ABAB* squares", *A*: Sb, Ge; *B*: Te) [5,11,21,22] act as nuclei for crystallization, aided by the higher cavity concentration and the presence of low-coordination Te atoms. Our work has then provided insight into the differences between Group 1 and 2 PC materials, which is related to their different crystallization mechanisms. Further study of the bond-interchange model is needed, and very large scale DF simulations should be possible in the near future.

REFERENCES

1. T. Matsunaga, J. Akola, S. Kohara, T. Honma, K. Kobayashi, E. Ikenaga, R. O. Jones, N. Yamada, M. Takata, and R. Kojima, "From local structure to nanosecond recrystallization dynamics in AgInSbTe phase change materials", Nature Mater. **10** (2011) 129.

2. M. Wuttig and N. Yamada, "Phase-change materials for rewriteable data storage", Nature Mater. **6** (2007) 824, and references therein.

3. Y. Fukuyama *et al.* "Time resolved investigation of nanosecond growth in rapid phase-change materials – Correlations with the rescording speed of digital versatile disc media", Appl. Phys. Expr. **1** (2008) 045001.

4. T. Matsunaga, Y. Umetani, and N. Yamada, "Structural study of a $Ag_{3.4}In_{3.7}Sb_{76.4}Te_{16.5}$ quadruple compound utilized for phase-change optical disks", Phys. Rev. B **64** (2001) 184116.

5. J. Akola, R. O. Jones, S. Kohara, S. Kimura, K. Kobayashi, M. Takata, T. Matsunaga, R. Kojima, and N. Yamada, "Experimentally constrained density-functional calculations of the amorphous structure of the prototypical phase-change material $Ge_2Sb_2Te_5$", Phys. Rev. B **80** (2009) 020201(R).

6. CPMD version 3.13. © IBM Corporation (1990-2010), © MPI für Festkörperforschung, Stuttgart (1997–2001) (http://www.cpmd.org).

7. J. P. Perdew, A. Ruzsinszky, G. I. Csonka, O. A. Vydrov, G. E. Scuseria, L. A. Constantin, X. Zhao, and K. Burke, "Restoring the density-gradient expansion for exchange in solids and surfaces", Phys. Rev. Lett. **100** (2008) 136406.

8. N. Troullier and J. L. Martins, "Efficient pseudopotentials for plane-wave calculations, Phys. Rev. B **43** (1991) 2006.

9. J. Akola and R. O. Jones, "Structure of liquid phase change material AgInSbTe from density functional/molecular dynamics simulations", Appl. Phys. Lett. **94** (2009) 251905.

10. O. Greben, P. Jóvári, L. Temleitner, and L. Pusztai, "A new version of the RMC++ Reverse Monte Carlo programme, aimed at investigating the structure of covalent glasses", J. Optoelectron. Adv. Mater. **9** (2007) 3021.

11. J. Akola and R. O. Jones, "Structural phase transitions on the nanoscale: The crucial pattern in the phase change materials $Ge_2Sb_2Te_5$ and GeTe", Phys. Rev. B **76** (2007) 235201; "Binary alloys of Ge and Te: order, voids, and the eutectic composition", Phys. Rev. Lett. **100** (2008) 205502; "Density functional study of amorphous, liquid and crystalline $Ge_2Sb_2Te_5$: Homopolar bonds and/or AB alternation?" J. Phys.: Condens. Matter **20** (2008) 465103.

12. M. L. Lee, L. P. Shi, Y. T. Tian, C. L. Gan, and X. S. Miao, "Crystallization behavior of $Sb_{70}Te_{30}$ and $Ag_3In_5Sb_{60}Te_{32}$ chalcogenide materials for optical media applications", phys. stat. sol. (a) **205** (2008) 340.

13. S. Kohara, K. Kato, S. Kimura, H. Tanaka, T. Usuki, K. Suzuya, H. Tanaka, Y. Moritomo, Matsunaga, N. Yamada, Y. Tanaka, H. Suematsu, and M. Takata, "Structural basis for the fast phase change of $Ge_2Sb_2Te_5$: Ring statistics analogy between the crystal and amorphous states", Appl. Phys. Lett. **89** (2006) 201910.

14. H. Tashiro *et al.*, "Structural analysis of Ag-In-Sb-Te phase-change material", Jpn. J. Appl. Phys. **41** (2002) 3758.

15. J.-J. Kim, K. Kobayashi, E. Ikenaga, M. Kobata, S. Ueda, T. Matsunaga, K. Kifune, R. Kojima, and N. Yamada, "Electronic structure of amorphous and crystalline $(GeTe)_{1-x}$ $(Sb_2Te_3)_x$ investigated using hard x-ray photoemission spectroscopy", Phys. Rev. B **76** (2007) 115124.

16. K. Shportko, S. Kremers, M. Woda, D. Lencer, J. Robertson, and M. Wuttig, "Resonant bonding in crystalline phase-change materials", *Nature Mater.* **7** (2008) 653.

17. B. Huang and J. Robertson, "Bonding origin of optical contrast in phase-change memory materials", Phys. Rev. Lett. **81** (2010) 081204(R).

18. D. Shakhvorostov *et al.*, "Evidence of electronic gap-driven metal-semiconductor transition in phase change materials", Proc. Nat. Acad. Sci. (US) **106** (2009) 10907-10911.

19. S. Caravati, M. Bernasconi, T. D. Kühne, M. Krack, and M. Parrinello, "Coexistence of tetrahedral- and octahedral-like sites in amorphous phase change materials", Appl. Phys. Lett. **91** (2007) 171906.

20. U.-C. Her, H. Chen, and Y.-S. Hsu, "Effects of Ag and In addition on the optical properties and crystallization kinetics of eutectic $Sb_{70}Te_{30}$ phase-change recording film", J. Appl. Phys. **93** (2003) 10097.

21. S. Caravati, M. Bernasconi, T. D. Kühne, M. Krack, and M. Parrinello, "Coexistence of tetrahedral- and octahedral-like sites in amorphous phase change materials", Appl. Phys. Lett. **89** (2007) 171906.

22. J. Hegedüs and S. R. Elliott, "Microscopic origin of the fast crystallization ability of Ge–Sb–Te phase-change memory materials", Nature Mater. **7** (2008) 399.

Biographies

J. Akola studied Physics at the Universities of Helsinki and Jyväskylä, Finland, obtaining his Ph.D. at Jyväskylä under Matti Manninen. After five years as a Post-doctoral Researcher at the Forschungszentrum Jülich, Germany, he returned in 2005 to the Nanoscience Center in Jyväskylä. He is currently Academy Research Fellow in the Tampere University of Technology, Finland, where he leads a group in Molecule and Materials Modeling. His fields of interest include classical, tight-binding, and density functional simulations of materials, nanoparticles, and biological systems.

R. O. Jones obtained his B.Sc. Hons (Physics) at the University of Western Australia in Perth and his Ph.D. at the University of Cambridge, England under Volker Heine. He spent three years as a Post-doctoral Associate at Cornell University before joining the Forschungszentrum Jülich. His main focus for over 30 years has been on density functional theory and its applications to a wide range of ordered and disordered systems (solids, surfaces, atomic clusters, molecules, polymers, biological molecules, …).